Turbulence, Heat and Mass Transfer 7

Caption in Fig. 2a and 4 corrected (in red)

Large Eddy Simulation of Heat Transfer in Boundary Layer and Backstep Flow Using PANS

L. Davidson[1]

Department of Applied Mechanics, Chalmers University of Technology, SE-412 96 Gothenburg, Sweden, lada@chalmers.se

Abstract — Developing boundary layer flow and the flow over a backward-facing step are studied here. The LRN PANS $k-\varepsilon$ [1] and the WALE turbulence model [2] are used as SGS models. The PANS (Partially Averaged-Navier-Stokes) modelling approach [3, 4] is a modified $k-\varepsilon$ model that can operate in both RANS and LES mode. An extension of PANS based on a four-equation $k-\varepsilon-\zeta-f$ model was recently proposed [5]. Synthetic, anisotropic, turbulent fluctuations are prescribed at the inlet to trigger the momentum equations into turbulence-resolving mode. The effect of the amplitude of the synthetic fluctuations is investigated. Different values of f_k are used. Two different discretization approaches are compared: 100% central differencing (CDS) or 95% CDS and 5% van Leer second-order bounded upwinding scheme. One 2D RANS simulation using the $k-\omega$ SST model is made for the backstep flow. A detailed comparison is made between 2D RANS and PANS including an analysis of the balancing terms in the momentum and temperature equations.

1. The LRN PANS $k-\varepsilon$ turbulence model

The Low-Reynolds-Number partially averaged Navier-Stokes (LRN PANS) turbulence model reads [1]

$$\frac{\partial k}{\partial t}+\frac{\partial \bar{u}_j k}{\partial x_j}=\frac{\partial}{\partial x_j}\left[\left(\nu+\frac{\nu_t}{\sigma_{ku}}\right)\frac{\partial k}{\partial x_j}\right]+P_k-\varepsilon$$

$$\frac{\partial \varepsilon}{\partial t}+\frac{\partial \bar{u}_j \varepsilon}{\partial x_j}=\frac{\partial}{\partial x_j}\left[\left(\nu+\frac{\nu_t}{\sigma_{\varepsilon u}}\right)\frac{\partial \varepsilon}{\partial x_j}\right]+C_{\varepsilon 1}P_k\frac{\varepsilon}{k}-C^*_{\varepsilon 2}\frac{\varepsilon^2}{k}$$

$$\nu_t=C_\mu f_\mu\frac{k^2}{\varepsilon}, C^*_{\varepsilon 2}=C_{\varepsilon 1}+\frac{f_k}{f_\varepsilon}(C_{\varepsilon 2}f_2-C_{\varepsilon 1}),\quad \sigma_k\equiv\sigma_k\frac{f_k^2}{f_\varepsilon},\quad \sigma_{\varepsilon u}\equiv\sigma_\varepsilon\frac{f_k^2}{f_\varepsilon}$$

$$\sigma_k=1.4,\sigma_\varepsilon=1.4,C_{\varepsilon 1}=1.5,C_{\varepsilon 2}=1.9,C_\mu=0.09,f_\varepsilon=1$$

In the baseline model, $f_k=0.4$. The damping functions are defined as

$$f_2=\left[1-\exp\left(-\frac{y^*}{3.1}\right)\right]^2\left\{1-0.3\exp\left[-\left(\frac{R_t}{6.5}\right)^2\right]\right\}$$

$$f_\mu=\left[1-\exp\left(-\frac{y^*}{14}\right)\right]^2\left\{1+\frac{5}{R_t^{3/4}}\exp\left[-\left(\frac{R_t}{200}\right)^2\right]\right\}$$

It may be noted that PANS is very similar to PITM [6] (Partially Integrated Transport Model); also in PITM the $C_{\varepsilon 2}$ coefficient is reduced when going into turbulence resolving mode.

2. Numerical method

An incompressible, finite volume code is used [7]. The convective terms in the momentum equations are discretized in two different ways: either pure central differencing (CDS) or 95% central differencing and 5% second-order bounded upwinding are used (van Leer [8]). Unless otherwise stated, the latter method is used.

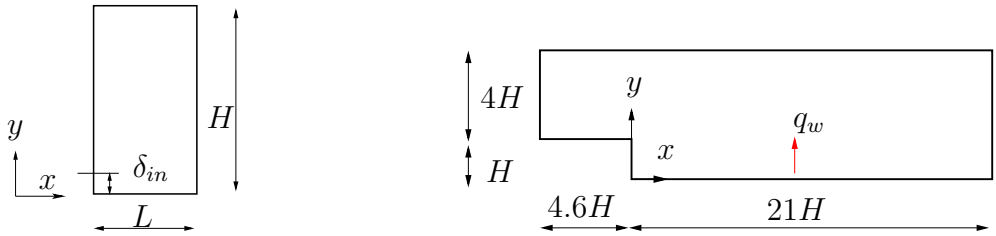

(a) Boundary layer flow. $L/\delta_{in} = 3.2$, $H/\delta_{in} = 15.6$, $Z_{max} = 1.5\delta_{in}$

(b) Backstep flow

Figure 1: Computational domains.

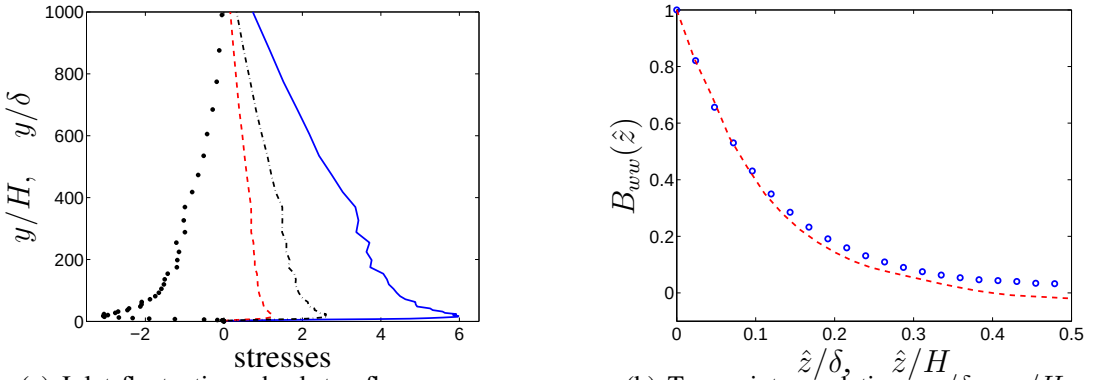

(a) Inlet fluctuations, backstep flow. ——: u^+_{rms}; - - -: v^+_{rms}; - · -: w^+_{rms}; ····: $\langle u'v'\rangle^+$.

(b) Two-point correlations. $y/\delta = y/H = 0.5$. ○: inlet; - - -: $x = 3\delta$.

Figure 2: Inlet fluctuation and two-point correlations for boundary layer and backstep flow.

3. Results

3.1. Boundary layer flow

The inlet Reynolds number is $Re_\theta = 3\,600$, which corresponds to $Re_\delta = U_{free}\delta_{in}/\nu \simeq 28\,000$. The inlet height, δ_{in}, see Fig. 1, is covered by 45 cells. The grid has $66 \times 96 \times 64$ cells in the streamwise (x), wall-normal (y) and spanwise (z) direction, respectively. A geometric stretching of 1.12 is used up to $y/\delta_{in} \simeq 1$; above this point, the stretching is 1.015. The height of the cell adjacent to the wall is $\Delta y = 0.00058\delta_{in}$. The inlet velocity is set to one, so that $\nu = 1/Re_\delta$.

A precursor RANS using the AKN model is carried out, from which U_{RANS}, V_{RANS} and k_{RANS} are obtained at $Re_\theta = 3\,600$. As an alternative, the inlet mean profile is taken from DNS [9]. The time-varying inlet velocities are then computed as $\bar{u}_{in} = U_{RANS} + u'_{synt}$, $\bar{v}_{in} = V_{RANS} + v'_{synt}$, $\bar{w}_{in} = w'_{synt}$, where $u'_{i,synt}$ denotes anisotropic synthetic fluctuations that were obtained using the same procedure as in [10]. In the present work, contrary to [10], the synthetic fluctuations are scaled with $k_{RANS}/k_{RANS,max}$. The inlet modelled turbulent kinetic energy and its dissipation are computed as $k_{in} = f_k k_{RANS}$, $\varepsilon_{in} = C_\mu^{3/4} k_{in}^{3/2}/\ell_{sgs}$, $\ell_{sgs} = C_s\Delta$, $\Delta = V^{1/3}$ [10]. Different values of C_s are investigated; the baseline value is $C_s = 0.05$.

Figure 2a presents the resolved Reynolds stresses generated by the synthetic inlet fluctuations for the backstep flow and the boundary layer flow. The two-point correlations at the inlet and at $x = 3\delta$ are shown in Fig. 2b; the integral length scale was set to $0.2\delta_{in}$ when the inlet

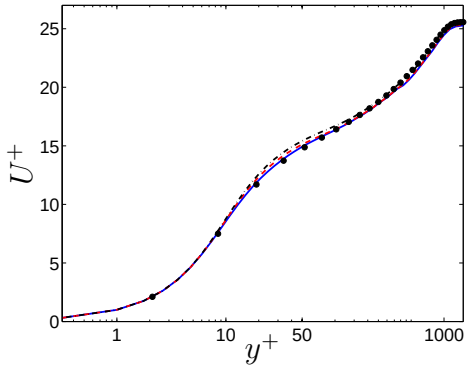

(a) 100% CDS. ——: $x = \delta_{in}$; - - -: $x = 2\delta_{in}$; - · -: $x = 3\delta_{in}$; ■: DNS [9]

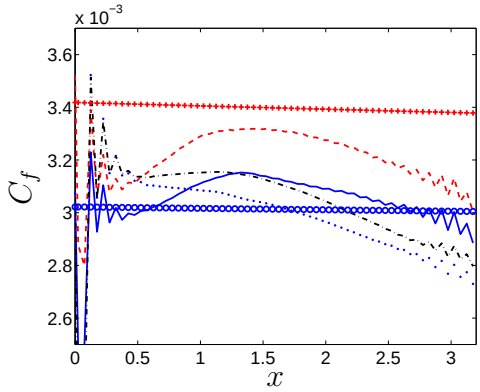

(b) ——: 100% CDS; - - -: 100% CDS, U_{in} from AKN; - - - -: 25% larger inlet fluctuations; ····: 25% larger inlet fluctuations, $C_s = 0.07$; markers: $0.37\,(log_{10}Re_x)^{-2.584}$.

Figure 3: Boundary layer. Skin friction and velocity profiles. Baseline: U_{in} from DNS.

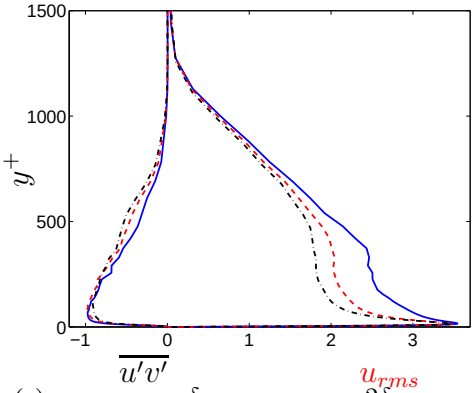

(a) ——: $x = \delta_{in}$; - - -: $x = 2\delta_{in}$; - · -: $x = 3\delta_{in}$.

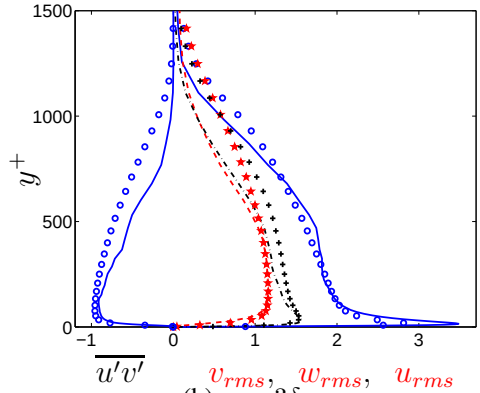

(b) $x = 3\delta_{in}$.

Figure 4: Boundary layer. Reynolds stresses. Markers: DNS [9]

fluctuations were generated which agrees well with the computed integral length scale.

The velocity profiles are presented in Fig. 3a at three different streamwise positions. The agreement with the DNS data [9] is very good. The skin friction also agrees well with experiments. Two sets of experimental C_f are shown: the inlet C_f is taken from the RANS AKN simulation for the upper red markers and from DNS for the lower markers. As can be seen, the RANS AKN model overpredicts the skin friction by some 12%. Note that the baseline values in Fig. 3b are 1) inlet mean profile from DNS, 2) $C_s = 0.05$ and 3) 95% CDS and 5% van Leer. As can be seen, the skin friction reaches a correct value within 5% at $x \simeq \delta$ for all cases. C_f decreases for $x > \delta$ because it is approaching its fully developed value, which is smaller than the theoretical value. This behavior is similar to that in fully developed flow [1], where the LRN PANS model predicts too high a centerline velocity, which is equivalent to too low a skin friction. The amplitude of the inlet fluctuations has only a small effect; as expected, large

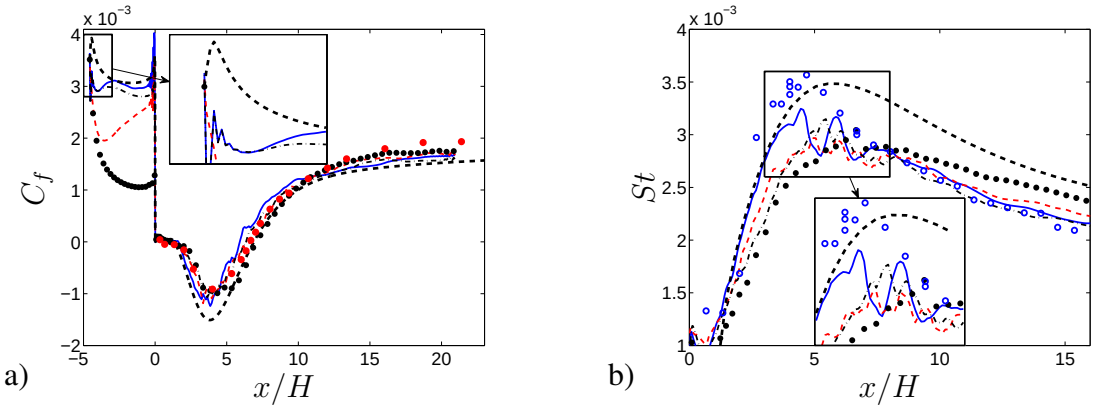

Figure 5: Backstep flow. Skin friction and Stanton number. —— : PANS; - - - : PANS, 50% smaller inlet fluctuations; - · - : WALE; •: PANS, no inlet fluctuations; - - - : 2D RANS; ○,●: experiments [11].

fluctuations generate large skin friction near the inlet. An increase of C_s from 0.05 to $C_s = 0.07$ (blue, dashed line) dampens the fluctuations. This is reasonable, since an increase in C_s gives a smaller inlet dissipation and hence a greater turbulent viscosity.

Figure 4 shows the resolved turbulent fluctuations. Baseline settings are used. The development can be seen in Fig. 4a; Fig. 4b shows the fluctuations at the end of the domain. It can be seen that, already at one boundary layer thickness downstream of the inlet, the predicted resolved turbulent fluctuations are quite reasonable. The agreement with DNS in Fig. 4b is good, although the predicted fluctuations are somewhat too low for $y^+ > 600$.

3.2. Backstep flow

The Reynolds number is $Re_H = 28\,000$, and the experiments were carried out by Vogel & Eaton [11]. The grid has $336 \times 152 \times 64$ cells in the streamwise (x), wall-normal (y) and spanwise (z) directions, respectively (see Fig. 1b). The step is covered by 96×52 cells in the streamwise and wall-normal directions. The inlet boundary layers at the upper wall and the step are covered by 45 cells; the grid is stretched by 1.12 for $1 < y/H < 3$ (the same as in the boundary layer simulations); the grid above the step is symmetric around $y = 3H$. A constant grid spacing is used in the x direction in $-4.6 < x/H < -0.27$ with $\Delta x/H \simeq 0.05$ (the same as in the boundary layer simulations); the grid is geometrically compressed by 0.89 in the region $-0.27 < x/H < 0$. The extent of the domain in the spanwise direction is $1.6H$. In the recirculation region, the mesh is taken from [12].

The inlet mean profile is taken from a 2D RANS AKN simulation (the same as in the boundary layer simulations). The inlet fluctuations are also the same as in Section 3.1. For the temperature, the inlet profile is $t = 0$ (constant in both space and time). At the lower wall, at $y = 0$, a constant heat flux, q_w, is set for $x > 0$. The inlet velocity is set to one, so that $\nu = 1/Re_H$.

LES simulations were carried out using PANS and WALE [2]. In most of the simulations, a 95% central differencing scheme (CDS) and 5% van Leer were used for the momentum equations; this is the baseline option. The influence of inlet fluctuations, 100% CDS and f_k will also be presented. The turbulent Prandtl number in the temperature equation was set to 0.7; the effect of reducing it to 0.4 will be shown. One RANS simulation using $k - \omega$ SST was also made; the turbulent Prandtl number was set to 0.9.

Figure 5 shows the skin friction and the Stanton number; profiles of the velocity and the streamwise resolved fluctuations are presented in Figs. 6 and 7. Without inlet fluctuations, we

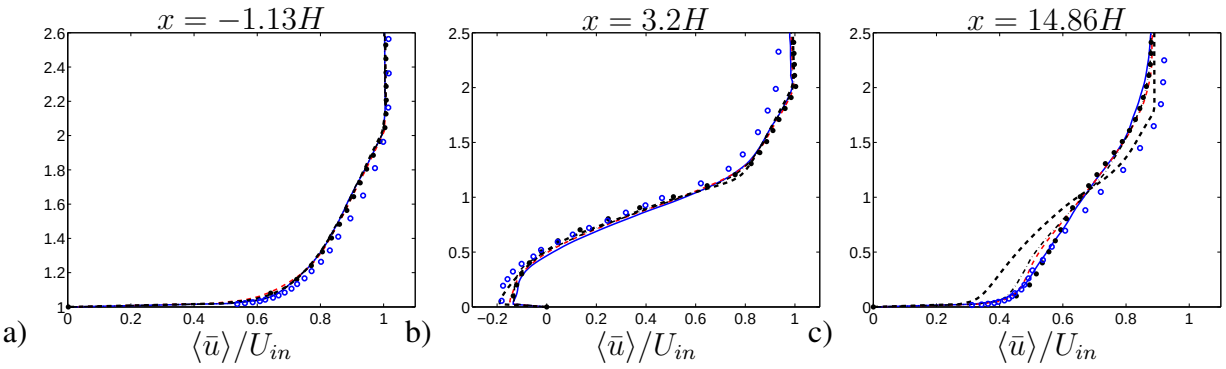

Figure 6: Backstep flow. Velocities. For legend, see Fig. 5.

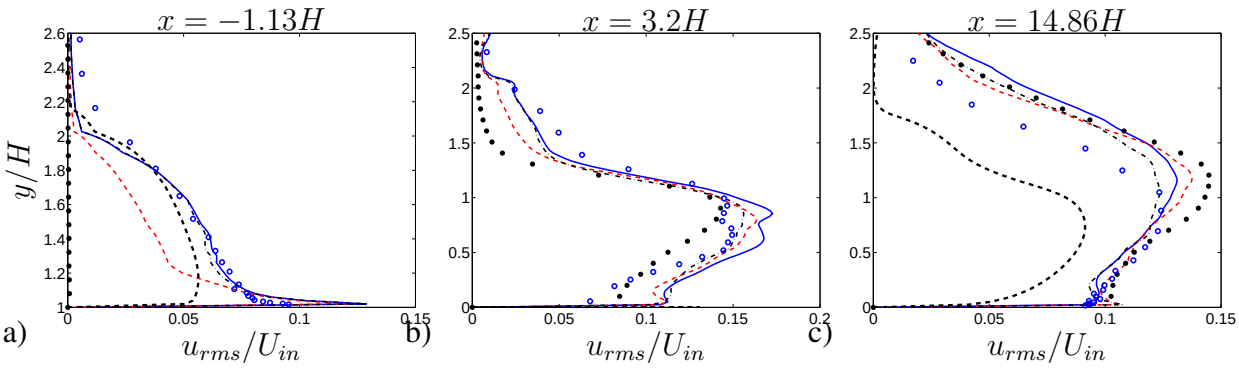

Figure 7: Backstep flow. Resolved streamwise fluctuations. For legend, see Fig. 5.

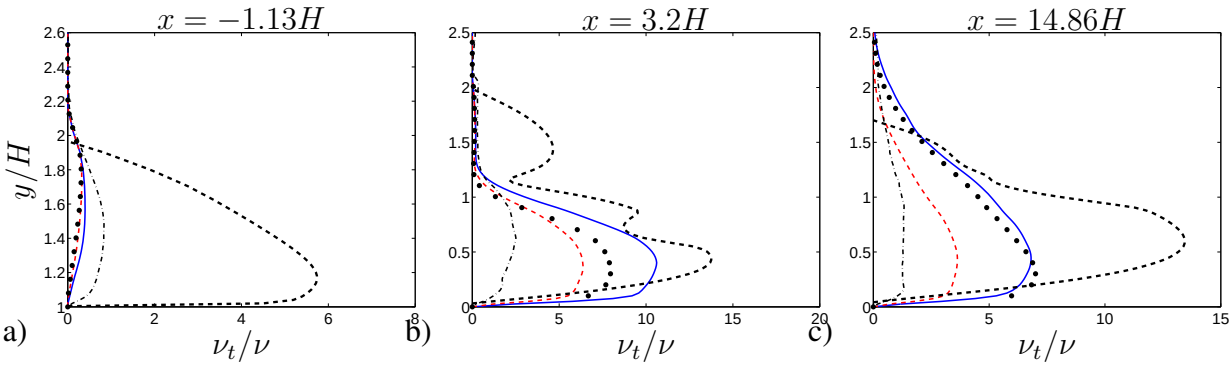

Figure 8: Backstep flow. Turbulent viscosity. —— : PANS; - - - : PANS, 50% smaller inlet fluctuations; - - - : WALE; •: PANS, no inlet fluctuations; - - - : 2D RANS (these values have been divided by a factor of 10).

obtain much too low a skin friction (Fig. 5a) and very small (virtually zero) resolved streamwise fluctuations (Fig. 7a) upstream of the step. The peak of the Stanton number is somewhat too small and too high downstream of the recirculation region.

The PANS and the WALE models give very similar results, but the Stanton number in the recirculation region is somewhat better predicted with the PANS model.

When the amplitude of the inlet fluctuations in the PANS simulations is reduced by 50%, the resolved fluctuations and the skin friction are, as expected, reduced upstream of the step. Otherwise, the amplitude of the inlet fluctuations has only a small effect on the predictions.

Two-dimensional RANS simulations were also carried out. The predicted recirculation is slightly too strong. The peak in the Stanton number is well captured, but the velocity profiles

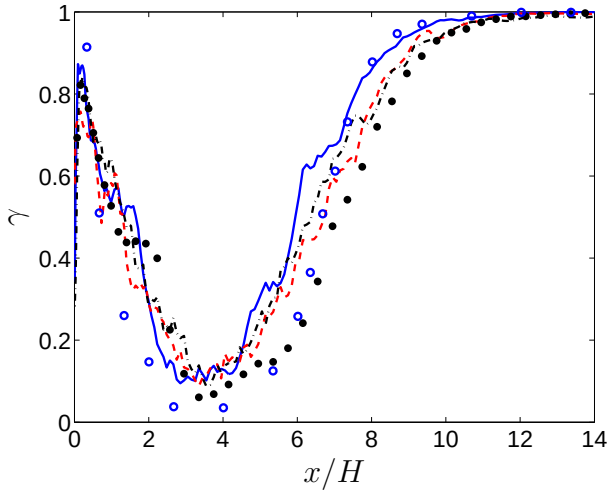

Figure 9: Fraction of time, γ, when the flow along the bottom wall is in the downstream direction. For legend, see Fig. 5.

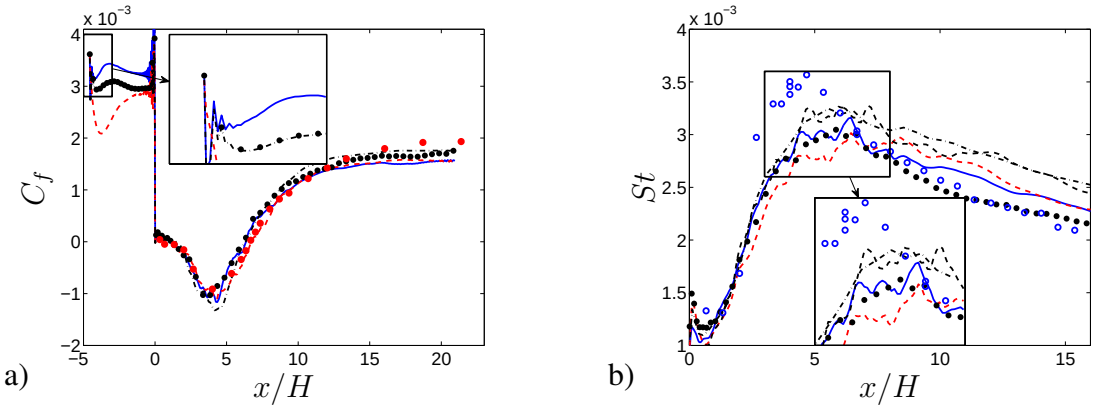

Figure 10: Backstep flow. Skin friction and Stanton number. PANS. —— : 100% CDS; - - - : 100% CDS, 50% smaller inlet fluctuations; •: $f_k = 0.3$; - · - : $f_k = 0.5$; - - - : $Pr_t = 0.4$; ○,●: experiments [11].

show that the recovery rate after the recirculation region is too slow; this is probably the reason for the too large St number in the recovery region.

Figure 8 presents turbulent viscosities (note that the RANS profiles have been scaled with a factor of 10). It can be seen that the RANS viscosities downstream the step are an order of magnitude larger than the LES values; upstream of the step they are more than two orders larger. The WALE model predicts a turbulent viscosity that is much smaller than the PANS model does.

Figure 9 shows the fraction of time when the flow at the bottom wall is positive, i.e. $\bar{u} > 0$. As can be seen, all simulations give similar results, the main difference being that the simulation without inlet fluctuations exhibits lower fraction of forward flow in the downstream part of the recirculation region. The agreement with experiment is good. It is interesting that even at the location of the strongest backflow ($x \simeq 3H$), the flow is during $5 - 10\%$ of the time in the downstream direction. At the reattachment point, $5.5H < x < 7H$, the fraction of time that the flow is in the positive x direction is approximately 50%. It can also be noted that immediately after the step ($x = 0$), the $\bar{u}$ velocity is positive during 80% of the time.

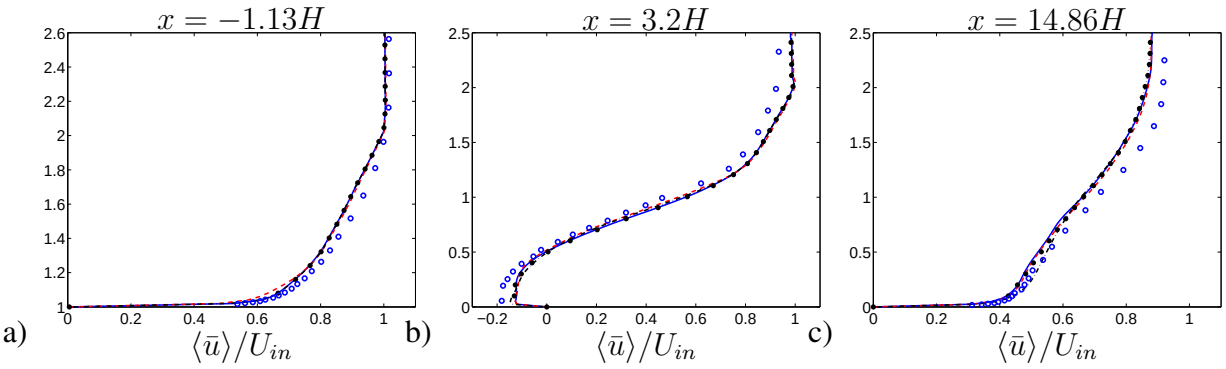

Figure 11: Backstep flow. Velocities. For legend, see Fig. 10.

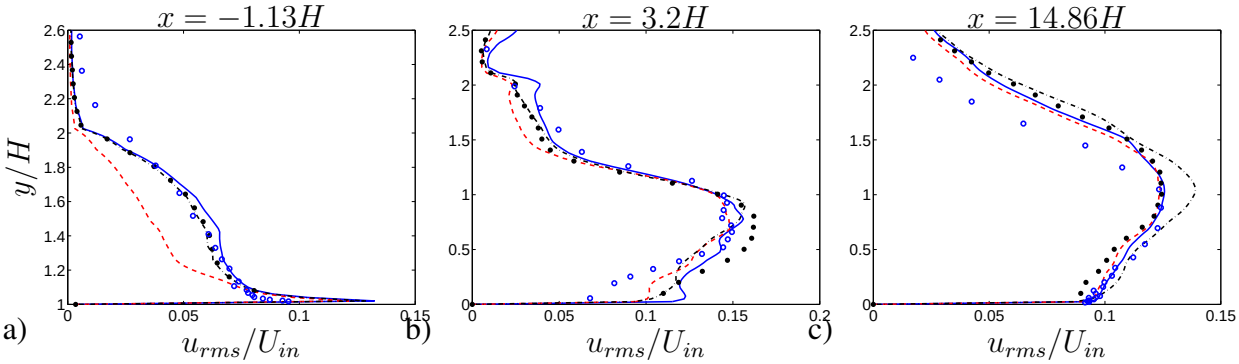

Figure 12: Backstep flow. Resolved streamwise fluctuations. For legend, see Fig. 10.

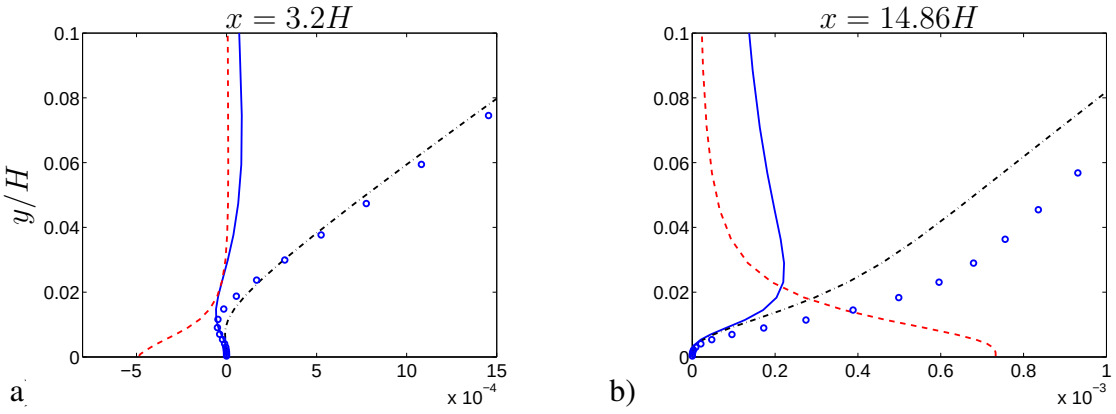

Figure 13: Backstep flow. Shear stresses. PANS. —— : $2\langle\nu_t\bar{s}_{12}\rangle$; - - - : $\nu\dfrac{\partial\langle\bar{u}\rangle}{\partial y}$; - · - : $-\langle\overline{u'v'}\rangle$; ○: $2\langle\nu_t\bar{s}_{12}\rangle - \langle\overline{u'v'}\rangle$.

Figures 10-12 show the influence of 100% CDS, f_k and turbulent Prandtl number. Because of smaller numerical dissipation, 100% CDS gives slightly larger resolved fluctuations and skin friction upstream of the step compared to 95% CDS and 5% van Leer, see Figs. 5 and 7. This results in a small displacement of the recirculation region and a small increase in the Stanton number. The effect of decrease/decrease in f_k is small, especially upstream of the step, where it has no effect at all. The reason is that the turbulent viscosity is very small upstream of the step, see Fig. 8. In the recirculation region, the change is f_k as expected: a larger/smaller f_k decreases/increases the resolved fluctuations because of larger/smaller turbulent viscosity. One

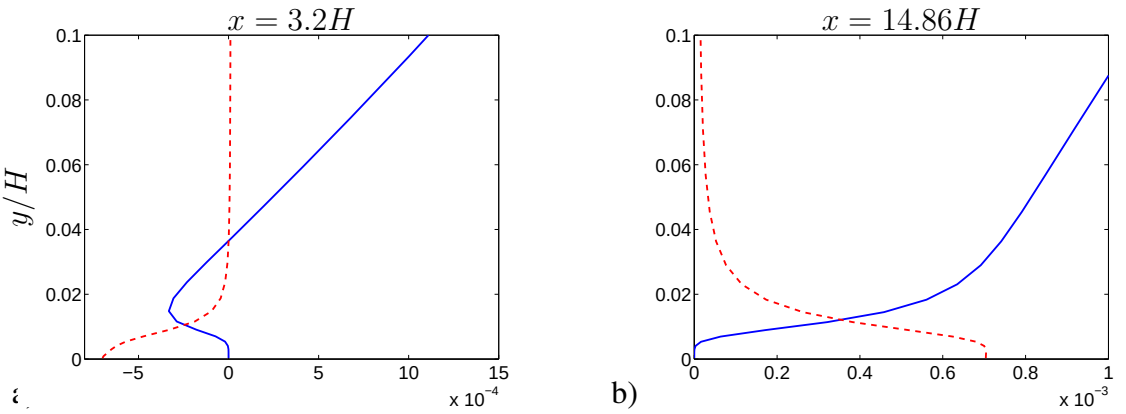

Figure 14: Backstep flow. Shear stresses. 2D RANS. For legend, see Fig. 13.

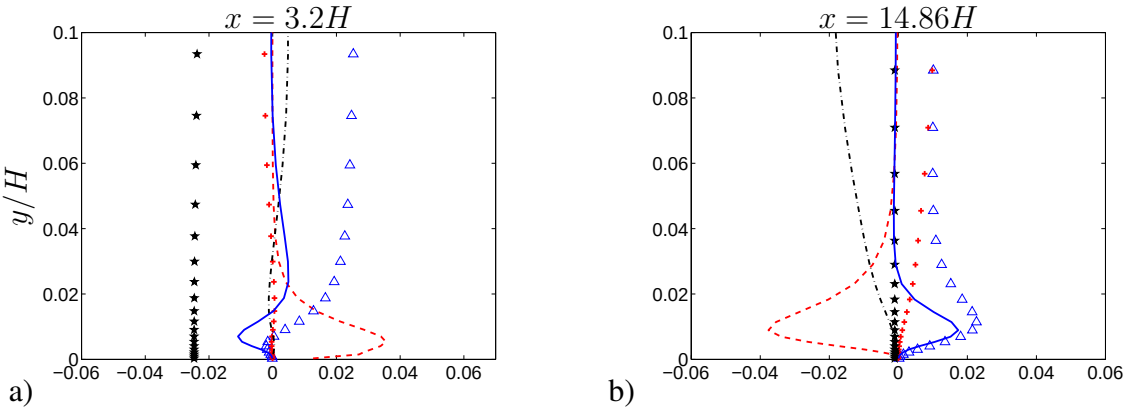

Figure 15: Backstep flow. Terms in the $\langle \bar{u} \rangle$ equation. PANS. —: $\dfrac{\partial}{\partial y}\left(2\langle \nu_t \bar{s}_{12} \rangle\right)$; - - -: $\nu \dfrac{\partial^2 \langle \bar{u} \rangle}{\partial y^2}$; -·-: $-\dfrac{\partial \langle \bar{u} \rangle \langle \bar{u} \rangle}{\partial x}$; +: $-\dfrac{\partial \langle \bar{u} \rangle \langle \bar{v} \rangle}{\partial y}$; ⋆: $-\dfrac{\partial \langle \bar{p} \rangle}{\partial x}$, △: $-\dfrac{\partial \langle \overline{u'v'} \rangle}{\partial y}$.

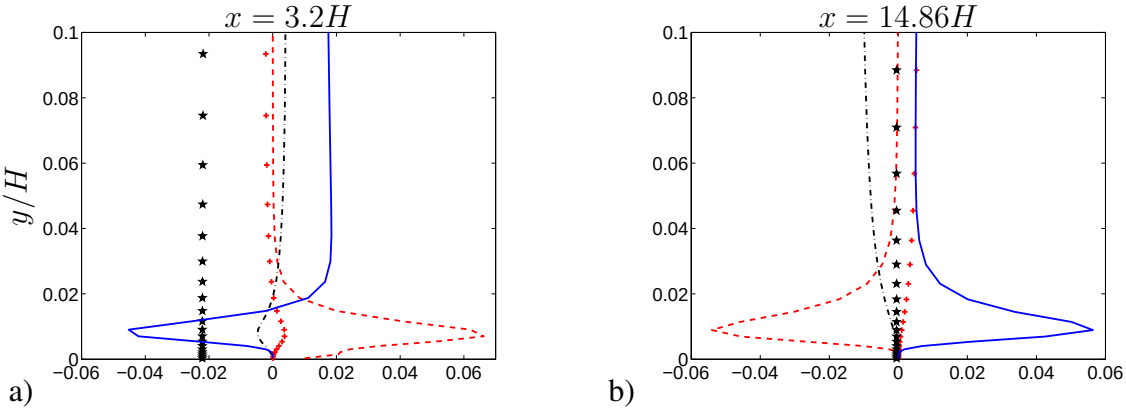

Figure 16: Backstep flow. Terms in the $\langle \bar{u} \rangle$ equation. 2D RANS. For legend, see Fig. 15.

simulation with a reduced Prandtl number (it is reduced from $Pr_t = 0.7$ to $Pr_t = 0.4$) is shown in Fig. 10b. As expected, the heat transfer is increased.

Figures 13-20 present some detailed comparisons between baseline PANS and 2D RANS. Figures 13 and 14 present the resolved, modelled and viscous shear stresses in the recirculation

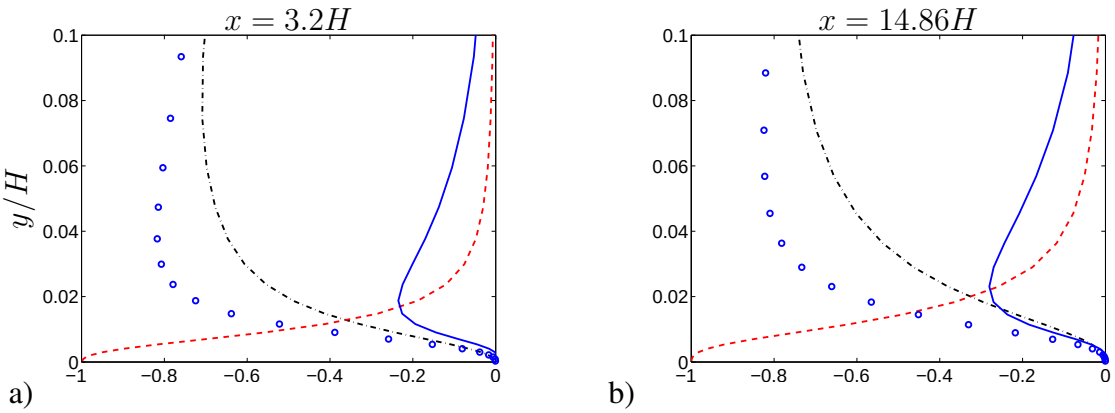

Figure 17: Backstep flow. Heat fluxes. PANS. —: $\left\langle \frac{\nu_t}{\sigma_t}\frac{\partial \bar{t}}{\partial y}\right\rangle$; - - -: $\frac{\nu}{\sigma_\ell}\frac{\partial \langle \bar{t}\rangle}{\partial y}$; - · -: $-\langle \overline{v't'}\rangle$. ○: $\left\langle \frac{\nu_t}{\sigma_t}\frac{\partial \bar{t}}{\partial y}\right\rangle - \langle \overline{v't'}\rangle$.

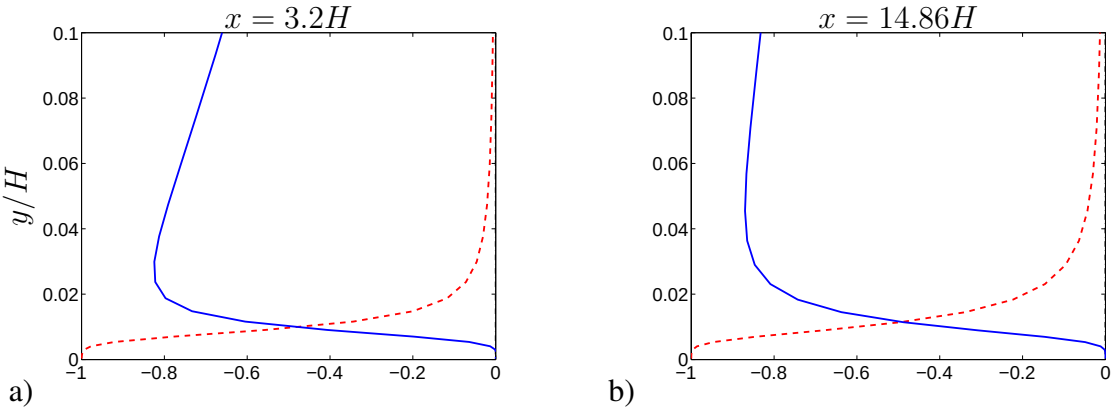

Figure 18: Backstep flow. Heat fluxes. 2D RANS. For legend, see Fig. 17

.

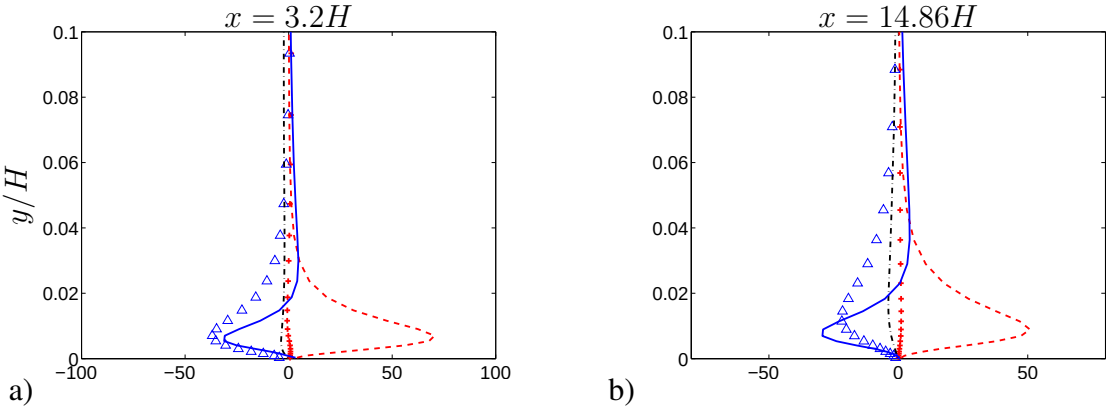

Figure 19: Backstep flow. Terms in the $\langle \bar{t}\rangle$ equation. PANS. —: $\frac{\partial}{\partial y}\left(\frac{\nu_t}{\sigma_t}\frac{\partial \langle \bar{t}\rangle}{\partial y}\right)$; - - -: $\frac{\nu}{\sigma_\ell}\frac{\partial^2 \langle \bar{t}\rangle}{\partial y^2}$; - - -: $-\frac{\partial \langle \bar{u}\rangle \langle \bar{t}\rangle}{\partial x}$; +: $-\frac{\partial \langle \bar{v}\rangle \langle \bar{t}\rangle}{\partial y}$; △: $-\frac{\partial \langle \overline{v't'}\rangle}{\partial y}$.

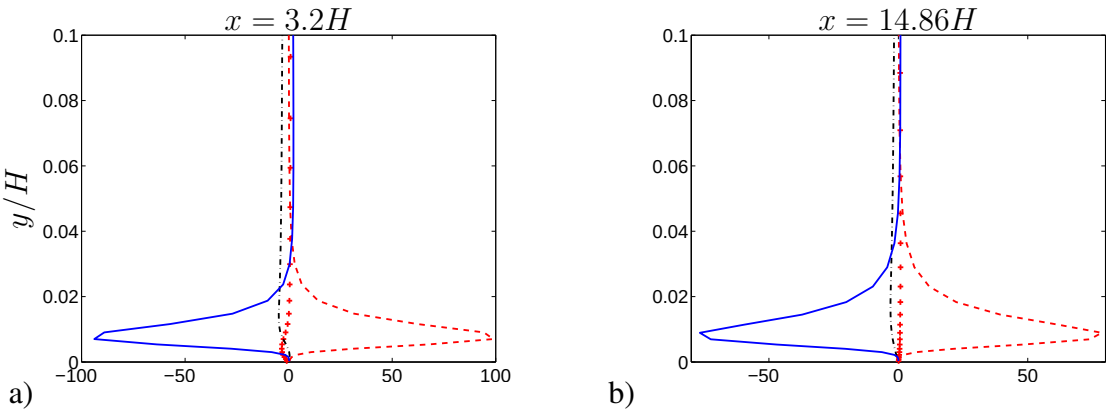

Figure 20: Backstep flow. Terms in the $\langle \bar{t} \rangle$ equation. 2D RANS. For legend, see Fig. 19.

region and the recovery region. It can be noted that the modelled turbulent shear stress obtained with the RANS simulation in the recirculation region has the wrong sign close to the wall ($y/H < 0.04$); the incorrect sign of the turbulent shear stress is also visible when comparing the balance terms in Figs 15a and 16a. The total shear stress predicted with the PANS model in the outer region is larger than that predicted with the RANS model, both in the recirculation region and in the recovery region. Looking at the turbulent shear stress in the recovery region, it can be seen that the boundary layer is thinner in RANS than in PANS. This explains why the turbulent diffusion terms are larger in RANS than in PANS (see Figs. 15b and 16b). The small turbulent shear stress predicted by RANS may explain the slow recovery rate and the thin boundary layer in the RANS simulation. It should be kept in mind, however, that it is not straightforward to compare predicted stresses in two simulations when the velocity fields are different; this difference in itself generates different turbulent shear stresses.

Figures 17 and 18 show the turbulent and viscous heat fluxes. A striking difference from the shear stresses in Figs. 13 and 14 is that the difference between the two locations (the recirculation region and the recovery region) is very small for the heat fluxes but large in the case of the shear stresses. The reason is of course that the heating of the lower wall creates temperatures that decrease for increasing y at all x. The velocity profiles have a much more irregular behavior because of the recirculation region. Furthermore, PANS and RANS predict heat fluxes that are much more similar than is the case for the shear stresses; however, it can be seen that the thermal boundary layer is thinner in RANS than in PANS. Because of the thinner thermal boundary layer, the gradients of the diffusion fluxes are much larger in RANS than in PANS. This is also seen by the terms in the temperature equation, see Figs. 19 and 20. Comparing the balance equations of velocity (Figs.15 and 16) and temperature (Figs.19 and 20), it can be seen that the contribution of the convective fluxes is much smaller in the temperature equation than in the velocity equation. The reason is probably that the convection terms in the velocity equation play an important role in balancing the pressure gradient.

4. Conclusions

LES has been made of boundary layer flow and backstep flow; the latter flow included heat transfer. The LRN PANS (with the baseline value $f_k = 0.4$) was used for both flows, and the WALE model was used for the backstep flow. Both models were demonstrated to give good agreement with experiments.

Synthetic anisotropic fluctuations were used to generate resolved turbulence near the inlet.

The sensitivity to their amplitude was investigated and it was found to be rather low. In the backstep flow, the synthetic fluctuations were omitted altogether in one simulation. As expected, the resolved turbulence upstream the step was zero, and the skin friction was much too low. However, downstream of the step, instabilities created resolved turbulence that was in surprisingly good agreement with experiments. Nevertheless, the predicted wall heat transfer was less well predicted compared to when synthetic inlet fluctuations were used.

Different values of f_k ($f_k = 0.3$ and 0.5) were used; the change in f_k was found to have only a small effect on the predictions.

The PANS backstep simulations were compared in some detail with 2D RANS using the $k-\omega$ SST model. It was found that the modelled turbulent shear stress in the RANS simulations was mostly smaller than the total (resolved and modelled) turbulent shear stress in the PANS simulations. The different terms in the velocity and temperature equation were analyzed. Near the wall, the turbulent shear stress balanced the viscous shear stress; the streamwise pressure gradient played a rather important role in the recirculation region, but it was smaller than the diffusion terms. Next, the diffusion terms (viscous and turbulent heat fluxes) in the temperature equation were analyzed. It was found that the terms in the PANS simulation and the RANS simulation were much more similar than in the velocity equation. As was the case for the velocity equation, the diffusion terms (viscous and turbulent heat fluxes) were the largest terms. One difference, however, was that the convection terms were much smaller in the temperature equation than in the velocity equation. The reason is probably that, in the velocity equation, the convection terms have to support the diffusion terms to balance the pressure gradient.

As mentioned above, PANS and WALE give very similar results, both in mean flow and resolved fluctuations. Nevertheless, the predicted turbulent viscosities differ rather much (PANS gives values which are more than a factor of five larger than WALE). The similarity in predicted results makes sense in one aspect: the modelled turbulence is negligible (except in the near-wall region) compared to the resolved turbulence. On the other hand it is somewhat surprising that the flow is that insensitive to the turbulent viscosity, because the SGS dissipation predicted by the two models should also – as the turbulent viscosity – differ by a factor of five.

Acknowledgments

The financial support of SNIC (the Swedish National Infrastructure for Computing) for computer time at C3SE (Chalmers Center for Computational Science and Engineering) is gratefully acknowledged. The initial grid for the backstep flow was provided by the group of Prof. Strelets in St. Petersburg. The project was financed by EU project ATAAC (Advanced Turbulence Simulation for Aerodynamic Application Challenges), Grant Agreement No. 233710.
`http://cfd.mace.manchester.ac.uk/ATAAC/WebHome`

References

1. J. Ma, S.-H. Peng, L. Davidson, and F. Wang. A low Reynolds number variant of Partially-Averaged Navier-Stokes model for turbulence. *International Journal of Heat and Fluid Flow*, 32:652–669, 2011.
2. F. Nicoud and F. Ducros. Subgrid-scale stress modelling based on the square of the velocity gradient tensor. *Flow, Turbulence and Combustion*, 62:183–200, 1999.
3. S.S. Girimaji. Partially-averaged Navier-Stokes model for turbulence: A Reynolds-averaged Navier-Stokes to direct numerical simulation bridging method. *ASME Journal of Applied Mechanics*, 73(2):413–421, 2006.

4. S.S. Girimaji, E. Jeong, and R. Srinivasan. Partially-Averaged Navier-Stokes method for turbulence: Fixed point analysis and comparison with unsteady partially averaged Navier-Stokes. *ASME Journal of Applied Mechanics*, 73(2):422–429, 2006.
5. B. Basara, S. Krajnović, S. Girimaji, and Z. Pavlović. Near-wall formulation of the Partially Averaged Navier Stokes turbulence model. *AIAA Journal*, 49(12):2627–2636, 2011.
6. R. Schiestel and A. Dejoan. Towards a new partially integrated transport model for coarse grid and unsteady turbulent flow simulations. *Theoretical and Computational Fluid Dynamics*, 18:443–468, 2005.
7. L. Davidson and S.-H. Peng. Hybrid LES-RANS: A one-equation SGS model combined with a $k-\omega$ model for predicting recirculating flows. *International Journal for Numerical Methods in Fluids*, 43:1003–1018, 2003.
8. B. van Leer. Towards the ultimate conservative difference scheme. Monotonicity and conservation combined in a second order scheme. *Journal of Computational Physics*, 14:361–370, 1974.
9. P. Schlatter and R. Orlu. Assessment of direct numerical simulation data of turbulent boundary layers. *Journal of Fluid Mechanics*, 659:116–126, 2010.
10. L. Davidson and S.-H. Peng. Emdedded LES with PANS. In *6th AIAA Theoretical Fluid Mechanics Conference, AIAA paper 2011-3108*, 27-30 June, Honolulu, Hawaii, 2011.
11. J.C. Vogel and J.K. Eaton. Combined heat transfer and fluid dynamic measurements downstream a backward-facing step. *Journal of Heat Transfer*, 107:922–929, 1985.
12. M. L. Shur, P.R. Spalart, M. Kh. Strelets, and A.K. Travin. A hybrid RANS-LES approach with delayed-DES and wall-modelled LES capabilities. *International Journal of Heat and Fluid Flow*, 29:1638–1649, 2008.